CORA Cork Open Research Archive
Cartlann Taighde Oscailte Chorcaí

Title	Development of residual stress in sol-gel derived Pb(Zr,Ti)O-3 films: An experimental study
Authors	Corkovic, S.;Whatmore, Roger W.;Zhang, Q.
Publication date	2008-04-16
Original Citation	Corkovic, S., Whatmore, R. W. and Zhang, Q. (2008) 'Development of residual stress in sol-gel derived Pb(Zr,Ti)O3 films: An experimental study', Journal of Applied Physics, 103(8), pp. 084101. doi: 10.1063/1.2890142
Type of publication	Article (peer-reviewed)
Link to publisher's version	http://aip.scitation.org/doi/abs/10.1063/1.2890142 - 10.1063/1.2890142
Rights	© 2008 American Institute of Physics, This article may be downloaded for personal use only. Any other use requires prior permission of the author and AIP Publishing. The following article appeared in Corkovic, S., Whatmore, R. W. and Zhang, Q. (2008) 'Development of residual stress in sol-gel derived Pb(Zr,Ti)O3 films: An experimental study', Journal of Applied Physics, 103(8), pp. 084101 and may be found at http://aip.scitation.org/doi/abs/10.1063/1.2890142
Download date	2026-11-05 09:05:28
Item downloaded from	https://hdl.handle.net/10468/4225

UCC
University College Cork, Ireland
Coláiste na hOllscoile Corcaigh

Development of residual stress in sol-gel derived $Pb(Zr, Ti)O_3$ films: An experimental study

S. Corkovic' , R. W. Whatmore, and Q. Zhang

Citation: Journal of Applied Physics **103**, 084101 (2008); doi: 10.1063/1.2890142
View online: http://dx.doi.org/10.1063/1.2890142
View Table of Contents: http://aip.scitation.org/toc/jap/103/8
Published by the American Institute of Physics



Development of residual stress in sol-gel derived $Pb(Zr,Ti)O_3$ films: An experimental study

S. Corkovic,[1,a)] R. W. Whatmore,[2] and Q. Zhang[1]
[1]*Department of Materials, Cranfield University, Bedfordshire MK43 0AL, United Kingdom*
[2]*Tyndall National Institute, University College Cork, Lee Maltings, Cork, Ireland*

(Received 30 August 2007; accepted 1 January 2008; published online 16 April 2008)

Residual stresses develop in the sol-gel-derived ferroelectric thin films during the transformation of the metal-organic gel to the metal oxide upon thermal treatment and due to the thermal and elastic mismatch between the $Pb(Zr_x,Ti_{1-x})O_3$ (PZT) film and the substrate materials during cooling. In this study, residual stresses were determined using the wafer curvature method after the deposition of multilayer PZT film on platinized (100) silicon wafers. A multilayer model for stress analysis was used to calculate the residual stress in PZT films of three different compositions: $x=0.4$, $x=0.52$, and $x=0.6$. Orientation dependent residual stresses were found in compositions containing the tetragonal phase, with $x=0.4$ and $x=0.52$. Depending on the fraction of (100) orientated domains low compressive or low tensile stress was found in $Pb(Zr_{0.4}Ti_{0.6})O_3$ (PZT 40/60). Higher residual stress was found in PZT films consisting of only rhombohedral crystallographic structure (PZT 60/40) while the residual stress in PZT films with morphotropic boundary composition (PZT 52/48) was significantly dependent on the film orientation and the phase composition and could range from 17 to 90 MPa. The effect of the film orientation on residual stress was found to be a function of the anisotropic thermal expansion coefficient of PZT. The contribution of the thermal and elastic properties of materials to the total wafer curvature was investigated and discussed. Finally, the residual stress results calculated with the four layer model were compared to the results calculated using the Stoney equation. © *2008 American Institute of Physics*. [DOI: 10.1063/1.2890142]

I. INTRODUCTION

Among the available ferroelectric materials, lead zirconate titanate $Pb(Zr_xTi_{1-x})O_3$ (PZT) is the most popular due to its superior dielectric, piezoelectric properties, and good thermal stability.[1] The applications of PZT films in microelectromechanical system (MEMS) devices exploiting the piezoelectric effect open up new possibilities in on-chip implementation.[2–4]

The demand of the residual stress characterization arises from the requirement of stress-free MEMS structures since the residual film stress can cause the device bending, as shown by Zhang *et al.*[5] The effects of residual stresses on the properties of thin films have been widely studied, for example, the effects of the residual stress on the ferroelectric and piezoelectric properties;[6–8] the effects of strain on the crystallographic orientation of the film when passing through the transition temperature;[9,10] the effects of applied stress on the ferroelectric properties;[11–14] and the effect of stress on the phase shift at the morphotropic phase boundary compositions.[15]

The residual stress characterization of chemical solution deposition (CSD) derived PZT thick films was a subject of many investigations, first reported for CSD derived thick films by Yi and Sayer.[16] The intrinsic stress develops in CSD films during heat treatment as a result of solvent evaporation and leads to the shrinkage of the film. The pyrochlore-to-perovskite transformation was associated with large stress[17] that accounts for the major fraction of the residual stress, around 100 MPa. Ong and Payne[18] investigated the stress during processing of single and multilayer films and showed that the values of residual stress in films at different PZT thicknesses were between 120 and 140 MPa. However, in their work PZT was deposited on silicon rather than on platinum. Spierings *et al.*[19] reported on the development of residual stress in the sol-gel deposited PZT 50/50 films and argued that the nature of stress in PZT is due to thermal expansion mismatch between PZT and the bottom (or the top) electrode which could be explained in more detail if the anisotropic thermal expansion of PZT is considered. The stress relaxation mechanism of the domain formation at the phase transition was first reported by Roitburd,[20] which was further developed by Speck and Pompe and co-workers[21,22] and Pertsev *et al.*[23] for epitaxial thin films by calculating the thermodynamically stable domain configuration dependent on the thermal strain difference between the film and the substrate. Roitburd and Kosenko[24] reported also on the orientation dependence of the elastic energy during phase formation which can be applied to the pyrochlore-perovskite transformation.

A detailed stress analysis in sputter deposited PZT films can be found in the work of Bruchhaus *et al.*[25–27] Bruchhaus *et al.* illuminated the stress development in the bottom electrode (Pt/TiO_2) and investigated the stress development during the pyrochlore-perovskite transformation in PZT films of various compositions.

The research activities regarding the residual stress characterization in PZT films and the influence of the stress on the electrical properties rapidly increased in the last few

a)Electronic mail: s.corkovic@cranfield.ac.uk.

 © 2008 American Institute of Physics

years. Although much work has focused on residual stress in CSD PZT films,[28,29] the understanding of the stress development that leads to residual stress is intermittent, particularly in the transition of the wet films to the crystallization. Further, to identify and design a stress-free device structure, it is important to identify the contribution of all layers to the total stress.

The purpose of this study is to shed light on the stress development during the whole processing of PZT film formation, from as-deposited wet film to its crystallization at high temperature and thereafter to cooling down to room temperature. It addresses the main stages at which the major stress can be developed or relaxed in CSD derived films. For this reason a nonconventional approach to stress calculation in thin films was adopted. This approach includes the stress calculation with a multilayer model where thermal and elastic properties of each layer are considered, the wafer curvature calculation modeling is comparative, or where otherwise not possible, stress calculation using the Stoney equation. Such analysis allowed identifying and separating the processes in the substrate and the PZT films which affect the residual stress in the PZT films.

II. EXPERIMENTAL

A. Wafer curvature measurement

Prior to any film processing the blank wafer displacement of all samples was measured using the Veeco Dektak surface profilometer. For some preliminary characterization of the wafer curvature the wafer displacement was measured in several equidistant and parallel lines across the wafer surface. The starting point for each scan was set along one line parallel to the primary flat of the wafer. Then the same wafer was rotated for 90° and the same kind of displacement measurement was performed in the direction perpendicular to the first set of scans. The scan length was always higher than 50% of the total diameter of the wafer.

For the residual stress characterization wafer curvature measurements were performed always along the same line across the wafer using a self-designed and constructed jig to assure the accuracy of the measurement. The wafer curvature was always measured on a blank wafer before platinum deposition, after platinum deposition, after platinum annealing, and after each PZT layer was completely crystallized.

B. Sol preparation

The sol precursor preparation and film processing were reported in detail in Ref. 17. Here, only a brief description will be given. Three different sol compositions were used: PZT 40/60, PZT 52/48, and PZT 60/40. The single layer thickness was 200 nm for all films. Thicker films (referred to as multilayer films) were fabricated by repeated spin coating. All films were processed at four distinct temperatures: 100, 300, 460, and 550 °C (or 630 °C for the PZT 60/40 films). The PbO sol was made by dissolving lead-2-ethylhexanoate in ethanol.

TABLE I. Samples' summary.

	PZT composition	Film thickness (μm)	Substrate	Wafer size (in.)	Orientation
Film 1	PZT 40/60	5	$Si/SiO_2/Pt$	2	(100)
Film 2	PZT 40/60	5	$Si/SiO_2/Pt$	2	(100)
Film 3	PZT 40/60	5	$Si/SiO_2/Pt$	2	(100)
Film 4	PZT 60/40	5	$Si/SiO_2/Pt$	2	(100)
Film 5	PZT 40/60	2	$Si/SiO_2/Pt$	2	Mixed (100)/(111)
Film 6	PZT 40/60	2	$Si/SiO_2/Pt$	4	Mixed (100)/(111)
Film 7	PZT 52/48	2	Si/Pt(200)	3	(100)
Film 8	PZT 52/48	2	Si/Pt/PbO	2	(100)
Film 9	PZT 52/48	3	$Si/SiO_2/Pt$	2	(111)
Film 10	PZT 52/48	4	$Si/SiO_2/Pt$	2	(111)

C. Substrate types

The PZT films were deposited on platinized silicon substrates. A Pt/Ti bilayer (100 nm/8 nm) was sputter deposited onto all substrates. Three different sizes of the silicon (100) substrates were employed: 2, 3, and 4 in. wafers. 2 in. silicon wafers were thermally oxidized to grow a 600 nm thick SiO_2 diffusion barrier layer. All other silicon wafers were commercially supplied with a 450 nm thick SiO_2 layer. In two samples only a native oxide layer was employed. Ten different samples were fabricated for the stress analysis. Their details are summarized in Table I.

D. Method for stress determination during PZT processing

For four experiments the wafer deflection was measured after heating the sample on a hotplate at given temperatures, in the temperature range between 100 and 550 °C. Each sample was heated, e.g., at 100 °C for 1 min and cooled down to room temperature followed by a wafer deflection measurement. The temperature of a hotplate was increased for 25 °C and the same cycle of heating the sample for 1 min, cooling it down to room sample and measuring the wafer curvature was performed until the last heating temperature (550 °C) was reached. Two experiments were performed on bare platinized silicon substrates; one substrate having an 8 nm thin Ti adhesion layer with following dimensions: $Pt/Ti/SiO_2/Si$ (100 nm/8 nm/ ~10 nm/525 μm) and the other substrate was identical expect for the Ti layer which was not deposited. For the two other experiments a single layer of PZT 40/60 (200 nm) was coated on the Pt/Ti/Si substrate, with the difference that one substrate was preannealed at 550 °C for 30 min and the other was not.

E. Crystallographic orientation

The orientation of each film was determined by the standard θ-2θ x-ray diffraction (XRD) method on a Siemens D5005 diffractometer using Cu $K\alpha$ radiation and a Goebel mirror. The peaks were deconvoluted and the integral intensities were determined for all detected peaks. The peak intensities were normalized according to Ref. 30 and compared

with the powder diffraction files from the PCPDF database. The crystallite size was determined using the Scherrer equation

$$\tau = \frac{\lambda k}{B_c \cos\theta}, \tag{1}$$

where τ is crystallite size, k is a parameter between 0.8 and 1, and B_c is full width at half peak maxima.

III. STRESS ANALYSIS METHODS

A. Model for composite structures

A model derived by Townsend *et al.*[31] was employed to calculate and analyze the curvature evolution and the residual stress from the curvature measurements in multilayer PZT films. This model was derived for composite structures and takes into account different mechanical and thermal expansion properties of each layer in composite structure. The details are given in Ref. 31, and here only the used equations are reproduced.

Based on the strength of materials approach the stress in each layer can be calculated using the following equation:

$$\sigma_i = E_i \left\{ -[\ln(d_{i,0}) + \alpha_i \Delta T] + \frac{\Sigma_j E_j t_j [\ln(d_{j,0}) + \alpha_j \Delta T]}{\Sigma_j E_j t_j} + (\pi - z)K \right\}, \tag{2}$$

whereby E_i, α_i, and t_i are the biaxial elastic modulus, the thermal expansion coefficient, and the thickness of the layer i, respectively; $d_{i,0}$ the length or diameter of the layer I before the temperature change ΔT, π the position of the neutral plane, K the composite curvature, and z the distance from the bottom of the composite structure to the top surface of the layer i. As stated in Ref. 31 it is required for all layers of the composite structure to have equal length at the point before the temperature changes. Whether such condition of the composite structure in PZT films exists or not will be discussed in the following sections.

Furthermore, this stress analysis approach allows curvature calculation by requesting a zero net moment and thus results in the following equation:

$$K = \frac{\Delta T \sum_i E_i \gamma_i (t_i/2) \left(-\alpha_i + \frac{\Sigma_j E_j t_j \alpha_j}{\Sigma_j E_j t_j} \right)}{\sum_i E_i t_i \left[\left(\frac{\pi t}{2} - \frac{t^2}{3} \right) + (t - \pi)\frac{\gamma_i}{2} - \frac{1}{12}(3\gamma_i^2 + t_i^2 - t^2) \right]}. \tag{3}$$

For details of Eq. (3), please see Ref. 31.

A residual stress model was designed to allow stress calculations in four layers, in particular, for the following structure: $Si/SiO_2/Pt/PZT$. The calculation of the stress in the silicon oxide layer was neglected if the silicon oxide was thinner than 50 nm. All required parameters for the calculations such as layer thickness and wafer length were measured except for the thermal expansion coefficients (TECs) and elastic moduli which were taken from diverse sources from the literature. The TECs for investigated PZT compositions were calculated using the thermal expansion data given in Refs. 32–34 for PZT 70/30, PZT 50/50, and PZT 48/52, respectively. The nonlinear thermal expansions for silicon, platinum, and silicon oxide were taken from Ref. 35. The TECs of all individual layers as used in the calculations are shown in Fig. 1 and their average values are summarized in Table I.

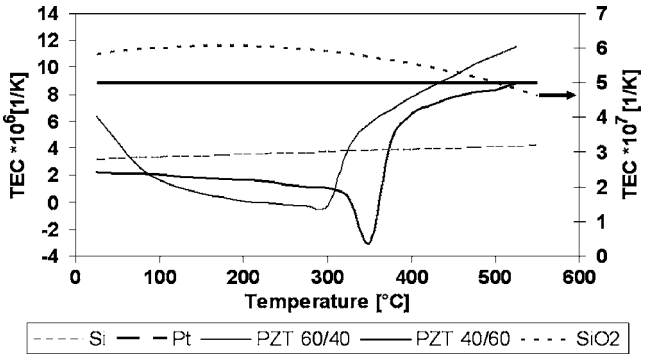


FIG. 1. Thermal expansion of Si, SiO_2, Pt, and PZT in the temperature range between the crystallization temperature of PZT 40/60 (550 °C) and room temperature (RT) as used for the residual stress calculation. The SiO_2 graph refers to the axes on the right.

The wafer curvature was calculated for every displacement measurement and in discrete points along the scan profile using

$$K(x) = \frac{y''}{(1 + y'^2)^{3/2}}, \tag{4}$$

where y' was a polynomial function of sixth order applied to the curvature profile. y' and y'' were first and second derivates of the function y.

B. Stoney equation

For some particular experiments it was not possible to calculate the stress via the model introduced in Sec. III A since the thermal or elastic properties are not known, e.g., of the wet PZT layer or where a nonelastic deformation was found, such as in platinum layer immediately after deposition. In this case the more common Stoney equation was applied

$$\sigma = (K_{\text{post}} - K_{\text{pre}}) \frac{E}{(1-\nu)} \frac{t_s^2}{6t_f}, \tag{5}$$

where K_{pre} and K_{post} are the wafer curvatures before and after the film, respectively; E, ν, and t_s the elastic modulus, Poison's ratio, and the thickness of the substrate, respectively, and t_f the film thickness. In addition, the residual stress results obtained with Eq. (2) were compared against the stress results calculated with the Stoney equation.[39]

IV. RESULTS AND DISCUSSION

A. Preliminary characterizations

The residual stress characterization based on the curvature measurement has been recently debated whether the film stress is isotropic and uniform as it is required when using,

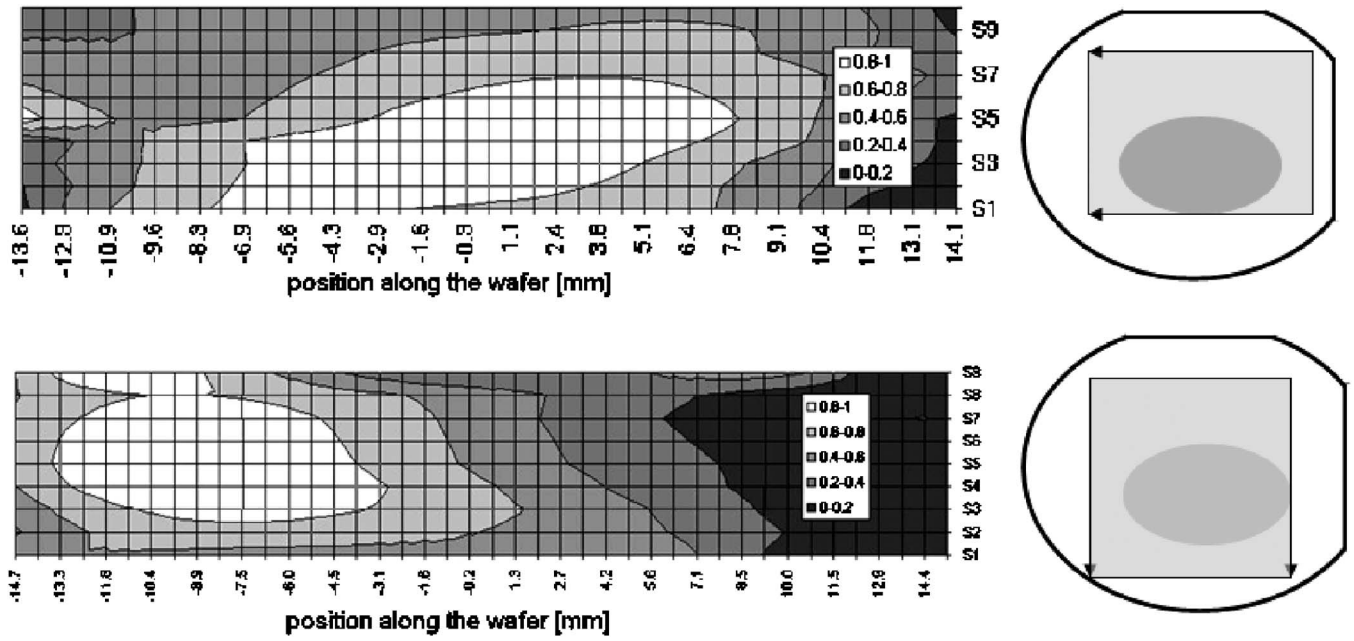


FIG. 2. Curvature of a 2 in. wafer after deposition of 1 μm thick PZT film. Two sets of measurements were performed according to Sec. II A, one perpendicular to the primary flat (above) and one set parallel to the primary flat (down). The wafer area for each measurement is depicted next to the graph, with the area of largest curvature marked in gray.

e.g., the Stoney equation[39] for stress calculation.[40–43] To calculate the residual stress from the wafer curvature measurements it is required to characterize the uniformity of the wafer curvature since both approaches to stress calculation, the Stoney equation and Eq. (2), are based on the linear and uniform beam deformations. Thus, strong deviations of curvature across the wafer surface can result in large differences in the stress values. To clarify the shape of the wafer bending due to film stress the curvature measurements were performed according to Sec. II A. Figure 2 shows the results of the normalized curvature of such scan for a 2 in. wafer after subtraction of the bare silicon wafer curvature. A cup shape of the wafer was observed and it showed a fairly radial bending of the platinized silicon wafer after a 1 μm thick PZT film was deposited. The cup shape was related to the anisotropic bending of the wafer indicating a nonuniform curvature. An area of the largest curvature was found slightly off the center of the wafer, most likely as a result of the shift of the center of gravity due to the primary and secondary flats on the wafer. However, the wafer deformation was much smaller compared to wafer thickness allowing the calculation of stress by Eq. (2) or Stoney equation. Thus, the residual stress analysis was restricted only to the area of the maximum curvature where maximum stress was found.

A similar experiment but on a 4 in. platinized silicon wafer was also conducted. After a 1 μm thick PZT film was deposited, the wafer bending showed a saddle shape (Fig. 3), indicating much more pronounced anisotropic bending of the substrate. Thus, strong variation of the curvature was found which makes the stress characterization more complicated when using the 4 in. wafer. Again, the stress calculation was limited to the central area of the wafer where the wafer curvature is fairly uniform. Nevertheless higher curvature and high stress can occur at some areas close to the edges of the wafer where the film cracking was sometimes observed when PZT was deposited onto a 4 in. silicon wafer.

B. Stress in the bottom electrode

To characterize the stress in the platinum bottom electrode the wafer curvature was measured before and after platinum deposition, and after substrate annealing at 550 °C for up to 30 min. The results are depicted in Fig. 4. It was found that the as-deposited platinum layer is under compressive stress and the stress changed from compressive to ten-

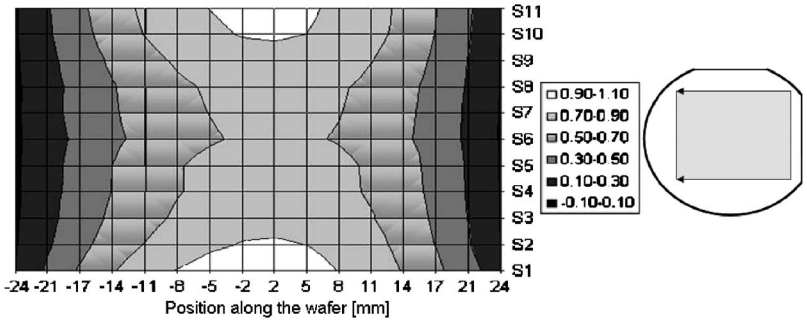


FIG. 3. Curvature of the 4 in. silicon wafer after the deposition Pt(100 nm)/Ti(8 nm) and 1 μm thick PZT film. Wafer geometry and the area of the measurement are represented in the image in the right.

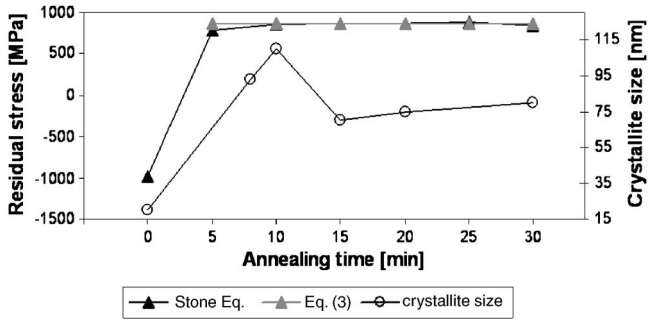


FIG. 4. Residual stress change and crystallite size after Pt/Ti sputter deposition and after annealing at 550 °C.

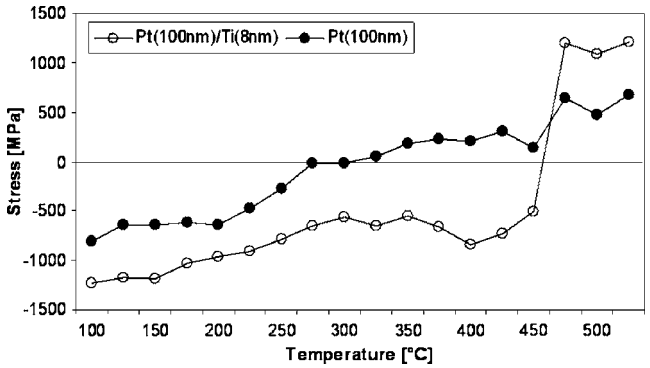


FIG. 5. Residual stress in Pt and Pt/Ti layer during stepwise thermal treatment in the temperature range between room temperature and 550 °C.

sile if platinum was annealed at 550 °C for around 5 min. Such results were reported earlier by several authors[44,45] where Pt(111) was sputter deposited at room temperature. Once the tensile stress was established in the platinum layer it did not change if the substrate was repeatedly annealed at the same temperature. Simultaneously, a platinum crystallite size increase was observed if platinum was annealed (Fig. 4). After the first 15 min of the annealing a crystallite size increase from 12 nm in average to around 100 nm was observed. After annealing for another 15 min a smaller grain size was observed, around 80 nm, suggesting a recrystallization of platinum, most likely driven by the defect density and compressive stress of the as-deposited platinum nanostructure as reported in Refs. 46 and 47. There was no noticeable crystallite size change upon further annealing at the same temperature. Thus, and alongside with the stress measurements after repeated annealing, it can be concluded that the platinum layer reaches a stable microstructure after the platinum recrystallization. This result is consistent to the results reported earlier by Ref. 48. The calculation of stress with the Stoney equation and Eq. (2) yielded similar result, around 870 MPa, suggesting that the stress at room temperature after annealing is entirely due to thermal expansion mismatch between Pt and Si.

Furthermore, there seems to be a relationship between the processes in the titanium layer, which is usually introduced as the adhesion layer between SiO_2 and Pt, and the stress relaxation (Fig. 5) as reported by Ref. 25. The experimental details for Fig. 5 are given in Secs. II A and II D and the stress was calculated using the Stoney equation. The substrate including the Ti adhesion layer showed higher compressive stress after sputter deposition than the substrate without the Ti layer. Upon subsequentially annealing the substrates the Pt only coated substrate showed a gradual change of stress from compressive to tensile while the Pt/Ti showed an abrupt change of stress at around 425 °C from compressive to tensile. Such abrupt change of stress in about the same temperature range was reported by Bruchhaus *et al.*[25] while oxidizing the Ti layer to TiO_2. Thus, the stress change in the bottom electrode during annealing has two contributions and can be associated with a Ti oxidation on one hand and with the platinum grain growth and recrystallization on the other hand.

C. Stress development during processing of the PZT film

The stress development in a 200 nm PZT 40/60 film on a preannealed and on an as-deposited substrate is depicted in Fig. 6. The details of the process characterization in the film are reported elsewhere.[17] The residual stress was calculated using the Stoney equation taking the wafer curvature of platinum as a reference whereby the PZT film thickness measurement was performed prior to every wafer curvature measurement with the same piece of equipment. The details of thickness reduction during processing are given in Ref. 49. One (Pt/Ti)/Si substrate was annealed for 30 min at 550 °C

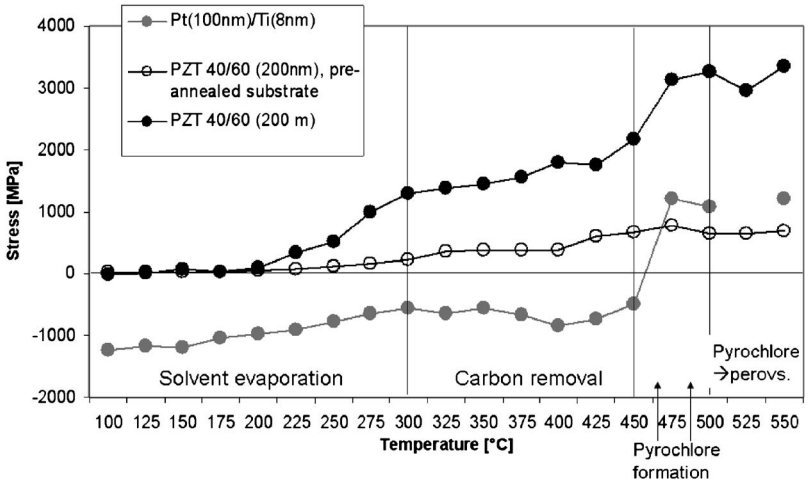


FIG. 6. Residual stresses in PZT 40/60 film deposited on an as-deposited and preannealed platinized substrate and in the bare platinized silicon substrate in the temperature range for PZT processing. Pt/Ti graph from Fig. 5 included.

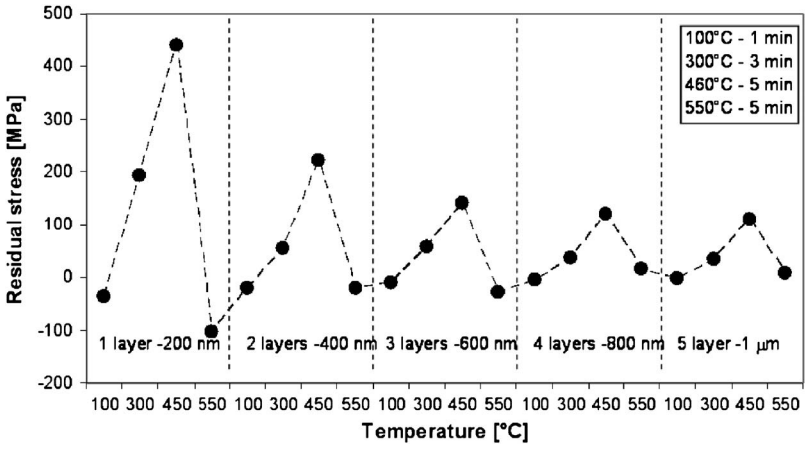


FIG. 7. Residual stress in multilayer PZT 40/60 film after each thermal processing step. The thermal profile is given in the text box. Five PZT layers were deposited.

before a PZT layer was spin coated and is referred to as the preannealed substrate. The graph from Fig. 5 on the stress evolution in annealed Pt is included for comparison.

Several stages during PZT processing can induce or relax strain. The first stage in the CSD processing is the stage of the solvents evaporation associated with large thickness shrinkage of the PZT film, usually at below 300 °C. However, only after the PZT film was treated at above 200 °C the tensile stress was forming in the PZT film. Based on the earlier findings reported in Ref. 49 a strong thickness shrinkage of the films was observed especially in the temperature range between 100 and 200 °C and further on, it was much larger than the lateral shrinkage. While the wet film can shrink to half of its thickness due to solvent evaporation there seems to be very little in-plane shrinkage probably as the film is constrained to the substrate. Above 300 °C and up to 450 °C the tensile stress was gradually increasing while the carbon and residual organics were removed from the film.

The next stage in the film processing related to stress generation is the pyrochlore formation, around 450–500 °C. The pyrochlore phase has much larger TEC than silicon or perovskite PZT,[11] and hence would induce large compressive strain while formed, as shown by Ref. 50. However, in the same temperature range the oxidation of Ti to TiO_2 from the substrate takes place, as mentioned in the previous section, and is superimposed with the stress stemming from the pyrochlore formation. This situation can be clearly observed in Fig. 6, where large tensile stress in a PZT film on as-deposited substrate was found but only a small stress increase in a film that was deposited on a preannealed substrate and where the underlying Ti layer was already oxidized.

Above 500 °C and thus in the next processing stage the stress in PZT films was not increasing. Here, the persovkite phase nuclei formation and crystallization take place and there are also a few possibilities of stress relaxation. The first one is related to the lattice match to the bottom layer. In case of the first deposited layer on Pt/Si there might form an intermetallic phase Pt_3Pb,[51] which reduces the lattice mismatch between PZT and Pt. Alongside the perovskite formation there is a change of TECs. This is the second strain-related step in the perovskite formation. The perovskite phase has a TEC between 9×10^{-6} and 11×10^{-6} K^{-1} (depending on the PZT composition) and thus larger than Pt or silicon. Therefore, if the film is under tensile stress at this point, some of the tensile stresses can be compensated due to large thermal expansion. The third possibility of stress relaxation is the domain formation when passing the phase transition temperature during cooling and will be discussed in more detail in the following section.

In general, a much higher and somewhat unrealistic stress was found in the PZT film that was spin coated on as-deposited platinum substrate. This is the result of the processes in the platinum bottom electrode that add up to the total PZT stress and can be easily mistaken for PZT stress if the substrate was not preannealed. The large final tensile stress in the film deposited on the preannealed substrate is due to incomplete crystallization as some pyrochlore was detected in the XRD (not shown here).

The residual stress in a multilayer PZT 40/60 film deposition after each thermal processing step is depicted in Fig. 7, after the platinum bottom electrode was sufficiently annealed. Five layers were deposited and the stress was calculated with the Stoney equation. It can be observed that tensile stress up to several hundred megapascal can build up in each layer, with the maximum stress during the pyrochlore formation, if the film is cooled down before the PZT film was completely crystallized. After the film was fully crystallized, after the thermal treatment at 550 °C, the residual stress decreased to −103 MPa for one PZT layer. With further layer deposition and full crystallization the residual stress decreased to around −20 MPa suggesting some stress relaxation with thickness increase.

D. Wafer curvature modeling

Before any stress calculation the wafer curvature was calculated using Eq. (3) for each sample and compared to the experimental results. The values from Table II were used for calculation except that the TEC of PZT had to be reduced in order to find a reasonable fit for the experimental data. The reason for this will be discussed in the next section. A four layer model was used for calculation consisting of $Si/SiO_2/Pt/PZT$ after the initial wafer curvature of bare SiO_2/Si wafer was subtracted in case the curvature was not measured after platinum annealing. It was found that the wafer curvature due to PZT film multilayer deposition was linear with increasing number of PZT layers. A curvature fit for

TABLE II. Average thermal and elastic properties for all layers in the temperature range between RT and 550 °C (or 630 °C for PZT 60/40).

Layer	Average TEC (1/K)	Biaxial Young's modulus (GPa)
Silicon (100)	3.6×10^{-6}[a]	180 in ⟨110⟩ direction[a]
Silicon oxide	5.5×10^{-7}[b]	77[a]
Platinum/ titanium	9×10^{-6}[b]	290[c]
PZT 40/60	3.7×10^{-6}	85[d]
PZT 52/48	5.3×10^{-6}	85[d]
PZT 60/40	4.7×10^{-6}	85[d]

[a]Reference 35.
[b]Reference 36.
[c]Reference 37.
[d]Reference 38.

three different samples (films 1–3) is depicted in Fig. 8 after the initial bare silicon wafer curvature and Pt/Ti curvature after annealing was subtracted. The difference between the samples lies in the preannealing conditions of the Pt/Ti layer, all other processing conditions such as layer thickness, PZT composition (PZT 40/60), and Pt and PZT deposition conditions were identical for all samples. First sample was annealed at 550 °C and the results of the stress before and after annealing were introduced earlier in Fig. 4. The second sample (film 2) had a Pt balance layer in such a way that the Pt/Ti layer of the same thickness was deposited on the front and back of the wafer to cancel out the stress from the platinum electrode. After the deposition of platinum to the back and front of the wafer the sample was annealed in the same way as film 1, Fig. 9. The third sample was identical to film 1 but was annealed at 700 °C (instead of 550 °C) for the same length of time, whereby no degradation of the bottom electrode was observed. The highest temperature for thermal treatment of PZT was 550 °C for all samples.

The linear regression was performed for all three samples. The calculation of the curvature for each sample was then compared to the linear regression curve of the experimental data. The least square linear regressions (r^2) for samples 1 and 2 were 0.83 and 0.96 whereby strong deviation from the linear behavior was observed for sample 3 (r^2=0.42). This deviation for the latter sample means that this sample is most likely not suitable for the curvature calculation using Eq. (3) and the reason might be some stress relaxation of the bottom electrode. The Pt stress in this

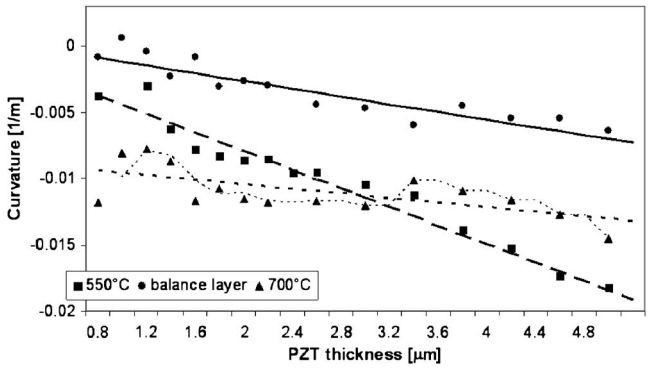


FIG. 8. Experimental and calculated curvature for three PZT films deposited on three differently prepared Pt/Si substrates after the substrate induced curvature was subtracted. The titles of the graphs refer to the annealing temperature of the substrate. The sample balance layer was annealed at 550 °C.

sample was stable after annealing at 700 °C but as the PZT film was crystallized at lower temperature it is likely that the bottom electrode was under tensile stress at 550 °C. This in turn could be a driving force for stress relaxation of Pt/Ti until the strain equilibrium of the bottom electrode to silicon substrate was reached at 550 °C. This change of stress contributes towards the total wafer curvature and is superimposed to the stress stemming from the PZT layer.

This can be explained if the stress in the bottom electrode is considered in more detail. It was concluded in the previous section that the platinum stress and microstructure were stable once the platinum was annealed for a sufficient length of time. This stable tensile stress state in platinum at room temperature suggests that the stress in platinum, initially due to defects and deposition stress, must have been minimized during annealing and eventually it is only a result of the thermal stress between Pt and Si as mentioned in the previous section. This, in turn, suggests that platinum and silicon must have similar planar dimensions at the annealing temperature and must be nearly strain-free. Since the Pt recrystallization is driven by strain and defect energy aiming to reduce the amount of strain and minimize the defect density, it is quite plausible to assume that after sufficient annealing time the strain can be reduced to a minimal level which would be at the point where the defect and strain energy is not sufficient to activate further grain growth. This energy equilibrium should lead to (nearly) strain-free platinum

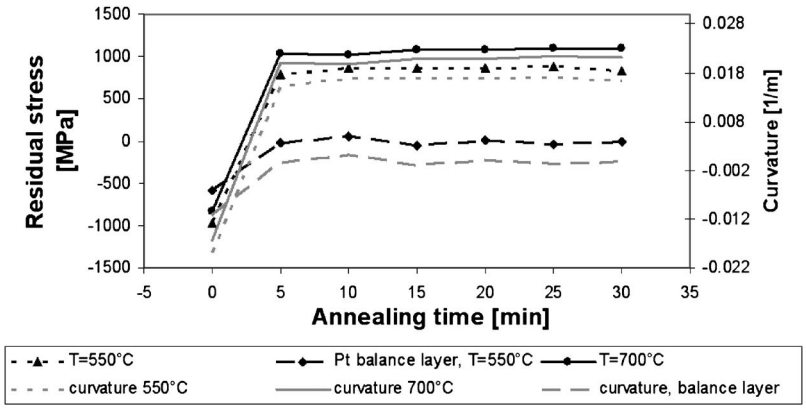


FIG. 9. Residual stresses and absolute curvature in the substrates before and after annealing, before the PZT films from Fig. 8 were deposited.

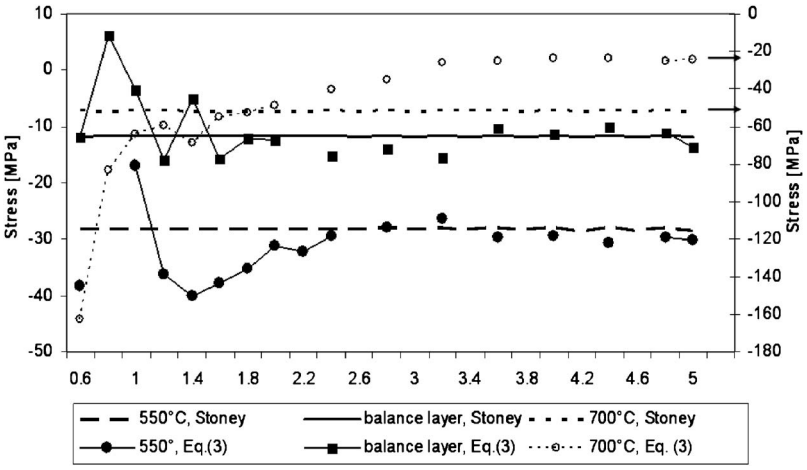


FIG. 10. Residual stress results for PZT films from Fig. 8 calculated with Stoney equation and Eq. (2).

which is only possible when the planar dimensions of the platinum and the substrate layer are (nearly) equal. Corresponding to this, the experimental evidence for stress-free Pt/TiO_2 electrode was reported by Bruchhaus *et al.*[25] in an *in situ* stress measurement showing the bottom electrode is nearly stress-free when close to the annealing temperature. Equal planar dimensions of the bottom electrode and silicon substrate at the annealing temperature are important for the stress or curvature calculations by Eqs. (2) and (4) in terms of the reference point for the calculation. It was mentioned in Sec. III A that for stress or curvature calculation in a temperature range ΔT there must be a reference temperature (T_1) at which all layers of the composite have equal length so that the curvature and stress change can be calculated from T_1 to any temperature T_2. Thus, in the case of annealed platinum on silicon there exists such reference temperature.

If PZT was deposited on such substrate the only strain in PZT film immediately before the treatment at the crystallization temperature must stem from the PZT layer itself. Thus, the planar dimensions of PZT layers at the reference temperature can be very different. Two different scenarios are possible after PZT crystallization—the first where all layers of the composite have equal planar dimensions including the PZT layer, and the second where the PZT layer planar dimension is smaller and it is thus under strain after the crystallization. Which scenario is more likely will depend on the crystallization kinetics of PZT. According to the investigations of the orientational dependence of elastic energy of solid state phase transformation from one phase into a second, coherent phase only such crystals are formed for which the elastic energy between the two phases is minimal,[24] provided the initial phase is strain-free. Supposed there is an additional term of the strain energy rising from the strain between the film and the substrate, other orientations for which higher elastic energy is required become possible and can be related to the strain energy at the crystallization temperature. The match of the film orientation to the substrate orientation can be realized by minimal deviations from the equilibrium. As the pyrochlore-to-perovskite transformation involves structural rearrangements of PZT and depending on the strain balance between PZT film and the substrate, it is quite possible that some or total accumulated strain in the film below the crystallization temperature can be relaxed during the crystallization and manifest in the appropriate orientation of the perovskite PZT film.

The stress results for all three films (films 1–3) were calculated with Eq. (2) and Stoney equation and are presented in Fig. 10. All films showed compressive stress. Above 2 μm thickness there is a good agreement of the results for films 1 and 2 calculated with either equation. Below this thickness there is a large deviation of the results when calculated with Eq. (2) and Stoney equation. This difference of the results is most likely due to the sensitivity of the Stoney equation to the ratio of film to substrate thickness, with Stoney equation being an approximation to the case of thin films on much thicker substrates and thus more sensitive when the thickness ratio is small. For the case of film 3 the results obtained with the Stoney equation differ greatly from the results obtained with Eq. (2). The reason for this was discussed in the previous paragraph and means that Eq. (2) cannot account for the stress that is due to plastic deformation of the substrate. It is also most likely that the crystallization temperature does not correspond to the reference temperature at which all composite layers have the same planar dimensions. From the stress results obtained with the Stoney equation it can be seen that the consequence of the substrate contribution to the stress, which could not be separated from PZT stress contribution, leads to apparently much higher PZT film stress within the first few PZT layers. With further PZT layer deposition the stress decreases strongly and is approximately constant with thickness increase if PZT is thicker than 3 μm.

E. Residual stresses in PZT films

The curvature calculation and stress calculation with Eqs. (2) and (4) were performed for all samples from Table I. The curvature was linear for all samples and the linear regression coefficient r^2 was 0.95 or better for all samples. A reasonably good match between the measured and calculated curvature was found for all samples except for the predominantly (100) oriented films where the TEC of PZT had to be reduced.

The residual stress results for films 3–10 from Table I are summarized in Table III. The stress in the platinum layer

TABLE III. Residual stresses and orientation in Si, SiO_2, Pt, and PZT films.

Sample	PZT composition	Film thickness (μm)	Orientation	Residual stress (MPa)			
				Si	SiO_2	Pt	PZT
Film 4	PZT 60/40	5	(100)	−1 to −4	−131	990	62
Film 5	PZT 40/60	2	Mixed (100)/(111)	Below 1	−115	860	10
Film 6	PZT 40/60	2	Mixed (100)/(111)	Below 1	−120	750	50
Film 7	PZT 52/48	2	(100)	−1	NA	862	19
Film 8	PZT 52/48	2	(100)	−1.6	NA	863	17
Film 9	PZT 52/48	3	Mixed (111)/(100)	−1.3	−115	860	56
Film 10	PZT 52/48	4	(111)	−4	−130	990	92

was only dependent on the PZT annealing temperature and was around 990 MPa for PZT 60/40 and around 860 MPa for PZT 40/60. In the silicon substrate and silicon oxide the compressive stress was found to be a few MPa and around −130 MPa, respectively.

In all PZT films the residual stress did not seem to be dependent on the PZT film thickness similar to the results of samples 1 and 2 from Fig. 10. The increase of stress was only fractional and within the experimental error.

This can be explained in the following way: When the first PZT layer is deposited, the film crystallizes on the substrate which can serve as a template for the film growth provided the lattice mismatch between the film and the substrate is low. During cooling the thermal and elastic stresses arise between the film and the substrate and account for the residual stress. When the second PZT layer is deposited on top of already crystallized PZT layer it can nucleate and grow in the same way as the first PZT layer. Thus, there is no component of lattice mismatch on the stress with additional layer deposition. As the thermal or elastic mismatch act only at the interfaces of layers with different properties there is only small residual stress increase due to total PZT thickness increase.

Among the comparable films, in terms of the same substrate and similar processing conditions (films 4, 5, and 10), the residual stresses in the PZT films were dependent on the PZT composition. PZT 52/48 was found to have the highest stress among the three compositions investigated in this study, which was around 90 MPa, followed by PZT 60/40 with 60 MPa, and the lowest in PZT 40/60 with around 10 MPa. Similar values for PZT 52/48 were reported by Refs. 13, 28, and 36 and lower values for PZT 40/60 by Ref. 52.

The influence of the substrate size could be observed in films 5 and 8 whereby the former film was deposited on a 2 in. wafer and the latter onto a 4 in. wafer. All other experimental parameters were identical. Thus the PZT 40/60 film deposited onto a larger wafer had much higher residual stress, around 50 MPa, compared to the 10 MPa on a smaller substrate.

Furthermore, large differences in the residual stresses in the PZT 40/60 and PZT 52/48 films with different orientations were found. Depending on the predominant (100) or (111) orientation PZT 40/60 films either compressive or tensile residual stress could have formed. The compressive residual stress in PZT 40/60 films was introduced in the previous section. The (100) oriented PZT 52/48 films showed tensile residual stress below 20 MPa for 2 or 3 μm thick films, while much higher residual stress (92 MPa) was found in (111) oriented PZT 52/48 films. A PZT 52/48 film with mixed (111) and (100) orientations showed residual stress around 56 MPa and thus in between the residual stress values for highly (100) and (111) oriented films.

The (100) oriented PZT 40/60 films were obtained by a certain thermal profile (not shown here) while for PZT 52/48 it was necessary to deposit the PZT films on a Pt(200)/Si substrate (film 7) or on a PbO (40 nm) coated Pt(111) substrate (film 8). Both films 7 and 8 were highly (100) oriented (Fig. 11). In both PZT 52/48 films the rhombohedral and tetragonal phases were found whereby the rhombohedral

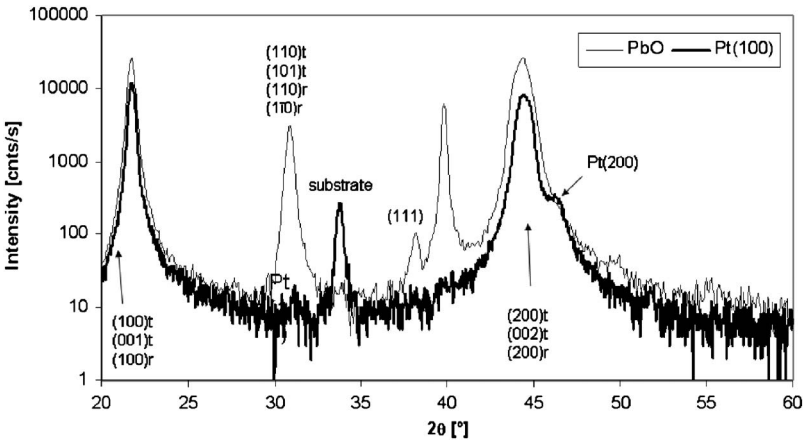


FIG. 11. X-ray diffractogram of film 4 [Pt(200)] and film 5 (PbO).

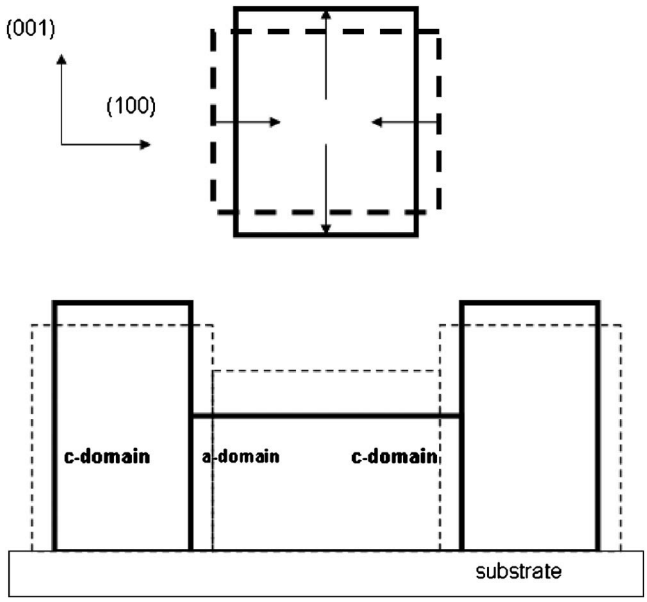


FIG. 12. The effect of the anisotropic expansion on the tetragonal PZT unit cell in (100) and (001) directions (above) and in the plane of the film (below).

phase accounted up to 18% in film 7 and around 30% in film 8, based on the ratio of the integral intensities as

$$r_{\text{rhombohedral}} = \frac{I_{(200)r}}{I_{(200)t} + I_{(002)t} + I_{(200)r}}. \quad (6)$$

Closer examination of the TECs of the tetragonal unit cell reveals that the TECs in (100) and (001) vary considerably.[34] According to the measurements of poled and unpoled tetragonal PZT by Cook *et al.*[34] the unit cell expands in *c*-direction and contracts in *a*-direction (Fig. 12). Thus, upon the phase transition from paraelectric to ferroelectric phase (upon cooling) the *a*-domains and *c*-domains are being formed, according to the stress at the Curie point as reported by Ref. 9. Upon further cooling, and in reference to the in plane of the film, the *a*-oriented domains lead to in-plane expansion while the *c*-domains lead to in-plane contraction. According to Cook *et al.* the average TEC is the sum of equal fractions of a_1-, a_2-, and *c*-domains as

$$\alpha = \frac{2\alpha_a + \alpha_c}{3} \quad (7)$$

with $\alpha_{a1} = \alpha_{a2}$. As a consequence of the strain at the Curie temperature and the *a*- and *c*-domain formation, the *a*- to *c*-domain ratio will dictate the average TEC of the film below the Curie temperature. The residual strain is then the sum of the amount of generated strain above the Curie temperature, the strain relaxation at the Curie temperature, and the strain below the Curie temperature.

In partially or completely (100) oriented PZT 40/60, for instance, the fraction of *a*-domains accounts to around 60% or more while the fraction of *c*-domains accounts to 30% or less. Due to the large fraction of *a*-domains-formed as a result of tensile stress at T_C-lower residual stress or even compressive stress can be found at the room temperature since the *a*-domains compensate for the tensile stress upon cooling. In addition to the TEC anisotropy of the tetragonal phase the morphotropic phase composition PZT 52/48 contains two phases-the tetragonal and the rhombohedral-which can influence the total TEC and this must be taken into account. The PZT 52/48 films can have two phases-the tetragonal and the rhombohedral. The phase field simulations for epitaxial PZT 52/48 films show that the phase formation in PZT 52/48 takes place gradually during cooling.[53] At first the tetragonal phase is being formed which can partly transform to a rhombohedral phase. Thus the total TEC of the (100) oriented PZT 52/48 films is the sum of the TEC of *a*- and *c*-oriented tetragonal domains and the (100) oriented rhombohedral phase. In total, the thermal contraction of (100) oriented PZT 52/48 films below the Curie temperature is lower than the contraction of silicon resulting in low tensile residual stress. This was estimated by using the TEC of the rhombohedral phase ($=8.4\times10^{-6}$ K^{-1}), the estimated fractions of the rhombohedral phase, and the ratio of *c*- to *a*-domains and their TEC, respectively. In (111) oriented PZT films, the same phase transition from paraelectric phase to ferroelectric phase is taking place at the Curie temperature; however, the efficient in-plane strain compensation below the Curie temperature must be much lower than that in (100) oriented films. Based on the TECs of the tetragonal phase and the unit cell parameters[54] the contraction of the (111) lattice plane in the plane of the film was estimated. The space diagonal of the tetragonal unit cell was calculated at the room temperature and at 300 °C using the anisotropic TECs in (100) and (001) directions, 4.7×10^{-6} and -6.6×10^{-6} K^{-1}, respectively, and the formula for space diagonal in a cuboid as follows:

$$d = \sqrt{a_1^2 + a_2^2 + c^2}. \quad (8)$$

The difference in the space diagonal between the 300 °C and the room temperature (RT) is the thermal expansion or contraction in the (111) direction upon heating or cooling between 300 °C and RT. From this calculation the TEC in (111) direction can be estimated to be around 8×10^{-6} K^{-1}. Thus, the thermal contraction of the tetragonal film below the Curie temperature in the (111) in-plane direction is much stronger and adds up to the tensile residual stress.

It was mentioned in Sec. IV D that in the case of the predominately (100) oriented films the TEC of PZT had to be reduced in order to find a good match between the experimental and calculated results. The change of the TECs affected only the slope of the linear graph by keeping the starting point of the initial curvature. After the discussion of the anisotropic TECs of PZT especially for (100) oriented films with the *a*/*c*/*a*-domain structure it becomes evident why lower TECs were more appropriate for the curvature calculation. However, the lower weighted average TEC can have other origins than the pure anisotropic TECs, e.g., due to the shifted T_C, according to the strain, to higher temperatures, as shown by Ref. 21 so that the large TEC of the paraelectric phase accounts for less of the total thermal strain. Further, it must be noted that the effect of the elastic anisotropy and especially for the different PZT compositions should be considered in terms of different elastic biaxial moduli for differ-

ent compositions. However, this point was omitted due to the lack of data of elastic constants for different PZT compositions.

It is interesting to note that, except for predominately (100) films, a good match between experimental and modeled curvature was found. This, together with the reasonable match of residual stress calculated with Stoney equation and Eq. (2) in films above 2 μm thick, suggests that the stress in PZT is entirely due to thermal and elastic mismatch between PZT and the substrate during cooling and that all accumulated stress in the CSD derived wet layer is relaxed during the crystallization of PZT. The idea of PZT strain release during crystallization accounts for the growth of PZT films with other orientations than those dictated by the substrate, e.g., in the case of (100) orientated PZT 40/60 films on Pt(111) substrate. If the same thermal processing profile was applied to PZT 52/48, the film showed predominant (111) orientation and thus the (100) orientation in PZT 52/48 films could only be produced by depositing the film on a Pt(200) substrate or such seeding layer, such as PbO, that supports the PZT (100) nucleation on Pt(111).

The result of the cubic perovskite orientation established during the crystallization further determines the strain in the film during cooling in the way that it can shift the transition temperature to other temperatures and can create an appropriate domain configuration.[21] Although the work in Ref. 21 was developed for sputtered epitaxial $PbTiO_3$ films a good agreement between this work and domain stability maps predicted by Ref. 21 was found for the predominant a-domain configuration in predominantly (100) oriented PZT 40/60 films and $a/c/a$ for PZT 40/60 films with mixed (111) and (100) orientation depending on the differential thermal expansion (film substrate).

V. CONCLUSIONS

In the present study the residual stress development in PZT films was investigated by means of wafer curvature measurements before and after the film deposition. The contribution of the substrate stress to the total stress was separately investigated and the change of stress during processing of one single layer or multilayer films was studied.

A combination of two equations, Eq. (2) and the Stoney equation, enabled a detailed residual stress analysis and Stoney equation was used to complement the results which could not be obtained by Eq. (2). On the other hand, if only Stoney equation was used for stress calculation, the origin and development of stress could not be analyzed in such detail as with Eq. (2). Both equations, where compared, yield similar results as expected.

A variety of PZT films, up to 5 μm thick, and three different PZT compositions were subject to stress analysis. Highest stress was found in (111) oriented PZT 52/48, up to 90 MPa; however, the residual stress was strongly orientation dependent. A very little increase of the residual stresses after the multilayer deposition of the films was found suggesting that there is practically no residual stress difference between 1 layer or 25 layer thick PZT film when using the Eq. (2).

A good match of the calculated and experimental curvature values, except for (100) oriented PZT 40/60 and PZT 52/48 films, suggested that the major fraction of the residual stress can be attributed to the thermal stress that developed during cooling of the film to the room temperature after the film was fully crystallized. Further, the curvature analysis revealed the impact of the orientation dependency on the stress which was attributed to the anisotropic thermal expansion of PZT relative to the silicon substrate, as a result of domain formation at the phase transition temperature. The effect of the anisotropic elastic properties of PZT was not considered since the elastic constants for investigated PZT compositions are not known.

ACKNOWLEDGMENTS

The financial support of EPSRC through Project Nos. GR/S45027/01 and EP/E035043/1 is gratefully acknowledged.

[1] S. Trolier-McKinstry and P. Muralt, J. Electroceram. **12**, 7 (2004).
[2] P. Muralt, IEEE Trans. Ultrason. Ferroelectr. Freq. Control **47**, 903 (2000).
[3] P. Muralt, J. Micromech. Microeng. **10**, 136 (2000).
[4] A. M. Flynn, L. S. Tavsrow, S. F. Bart, R. A. Brooks, D. J. Ehrlich, K. Udayakumar, and L. E. Cross, J. Microelectromech. Syst. **1**, 44 (1992).
[5] L. Zhang, J. Tsaur, and R. Maeda, Jpn. J. Appl. Phys., Part 1 **42**, 1386 (2003).
[6] W. C. Goh, K. Yao, and C. K. Ong, Appl. Phys. Lett. **87**, 072906 (2005).
[7] I. Chung, I. K. Yoo, W. Lee, C. W. Chung, and J. K. Lee, Integr. Ferroelectr. **10**, 99 (1995).
[8] K. Fujito, N. Wakiya, K. Shinozaki, and N. Mizutani, J. Ceram. Soc. Jpn. **110**, 421 (2002).
[9] B. A. Tuttle, J. A. Voigt, T. J. Garino, D. C. Goodnow, R. W. Schwartz, D. L. Lampa, T. J. Headley, and M. O. Eatough, Proceedings of the Eighth IEEE International Symosium on Applications of Ferroelectrics, New York, 30 August–2 September, 1992 (unpublished) p. 344.
[10] S. Y. Kweon, S. H. Yi, and S. K. Choi, J. Vac. Sci. Technol. A **15**, 57 (1997).
[11] T. J. Garino and H. M. Harrington, *Ferroelectric Thin Film II Symposia Mat. Res. Soc.*, MRS Symposia Proceedings No. 243 (Materials Research Society, Pittsburgh, PA, 1992), p. 341.
[12] J.-W. Lee, G.-T. Park, C.-S. Park, and H.-E. Kim, Appl. Phys. Lett. **88**, 072908 (2006).
[13] J. F. Shepard, Jr., S. Trolier-McKinstry, M. A. Hendrickson, and R. Zeto, ISAF 1996—Proceedings of the Tenth IEEE International Symposium on Applications of Ferroelectrics, East Brunswick, NJ, 1996 (unpublished), p. 161.
[14] S. S. Sengupta, S. M. Park, and D. A. Payne, Integr. Ferroelectr. **14**, 193 (1997).
[15] Q. Zhang, S. Corkovic, J. M. Marshall, C. P. Shaw, and R. W. Whatmore, Integr. Ferroelectr. **88**, 85 (2007).
[16] G. Yi and M. Sayer, in *Proceedings of the Eighth IEEE International Symposium on Applications of Ferroelectrics*, Greenville, SC, 1992, edited by M. Liu, A. Safari, A. Kingon, and G. Haerting (Institute of Electrical and Electronic Engineers, Piscataway, NJ, 1992), p. 289.
[17] S. Corkovic, Q. Zhang, and R. W. Whatmore, J. Electroceram. **19**, 295 (2007).
[18] R. J. Ong and D. A. Payne, Proceedings of the 2000 12th IEEE International Symposium on Applications of Ferroelectrics, 2001 (unpublished), Vol. 1, Pt. 1, p. 397.
[19] G. A. C. M. Spierings, G. J. M. Dormans, W. G. J. Moors, M. J. E. Ulenaers, and P. K. Larsen, J. Appl. Phys. **78**, 1926 (1995).
[20] A. L. Roitburd, Phys. Status Solidi A **40**, 333 (1977).
[21] J. S. Speck and W. Pompe, J. Appl. Phys. **76**, 477 (1994).
[22] S. K. Streiffer, C. B. Parker, A. E. Romanov, M. J. Lefevre, L. Zhao, J. S. Speck, W. Pompe, C. M. Foster, and G. R. Bai, J. Appl. Phys. **83**, 2742 (1998).
[23] N. A. Pertsev, A. G. Zembilgotov, and A. K. Tagantsev, Phys. Rev. Lett. **80**, 1988 (1998).
[24] A. L. Roitburd and N. S. Kosenko, Phys. Status Solidi A **35**, 735 (1976).

[25]R. Bruchhaus, D. Pitzer, R. Primig, W. Wersing, and Y. Xu, Integr. Ferroelectr. **14** 141 (1997).
[26]R. Bruchhaus, D. Pitzer, R. Primig, M. Schreiter, and W. Wersing, Integr. Ferroelectr. **21**, 467 (1998).
[27]R. Bruchhaus, D. Pitzer, M. Schreiter, and W. Wersing, J. Electroceram. **3**, 151 (1999).
[28]E. Hong, R. Smith, S. V. Krishnaswamy, C. B. Freidhoff, and S. Trolier-McKinstry, Thin Solid Films **10**, 213 (2006).
[29]J.-W. Lee, C.-S. Park, M. Kim, and H.-E. Kim, J. Am. Ceram. Soc. **90**, 1077 (2007).
[30]G. B. Harris, Philos. Mag. **43**, 113 (1952).
[31]P. H. Townsend, D. M. Barnett, and T. A. Brunner, J. Appl. Phys. **62**, 4438 (1987).
[32]B. Noheda, J. A. Gonzalo, J. De Frutos, A. Gonzalez, and C. Moure, J. Mater. Sci. Lett. **16**, 101 (1997).
[33]D. R. Biswas, S. Chandratreya, and J. A. Pask, Ceram. Bull. **98**, 792 (1979).
[34]W. R. Cook, Jr., D. A. Berlincourt, and F. J. Scholz, J. Appl. Phys. **34**, 1392 (1962).
[35]L. B. Freud and S. Suresh, *Thin Film Materials: Stress Defect Formation and Surface Evolution* (Cambridge University Press, Cambridge, 2003), p. 92.
[36]I. Chung, I. K. Yoo, W. Lee, C. W. Chung, and J. K. Lee, Integr. Ferroelectr. **10**, 99 (1995).
[37]W. Dax, K. Grundelfinger, W. Häffner, H. Itschner, G. Kotsch, and M. Staniczek, *Tabellenbuch für Metalltechnik* (Handwerk und Technik, Hamburg, 1991).
[38]Y. C. Zhou, Z. Y. Yang, and X. J. Zheng, Surf. Coat. Technol. **162**, 202 (2003).
[39]G. G. Stoney, Proc. R. Soc. London, Ser. A **82**, 172 (1909).
[40]I. A. Blech, I. Blech, and M. Finot, J. Appl. Phys. **97**, 113525 (2005).
[41]R. L. Engelstad, Z. Feng, E. G. Lovell, A. R. Mikkelson, and J. Sohn, Microelectron. Eng. **78–79**, 404 (2005).
[42]R. Clos, A. Dadgar, and A. Krost, Phys. Status Solidi A **201**, R75 (2004).
[43]C. A. Klein, J. Appl. Phys. **88**, 5499 (2000).
[44]E. Defay, C. Malhaire, C. Dubois, and D. Barbier, *Thin Film Stresses and Mechanical Properties VIII Symposium*, MRS Symposia Proceedings No. 594 (Materials, Research Society, Pittsburgh, PA, 2000), p. 237.
[45]L. Zhang, M. Ichiki, and R. Maeda, J. Eur. Ceram. Soc. **24**, 1673 (2004).
[46]S. Y. Kweon, S. K. Choi, S. J. Yeom, and J. S. Roh, Jpn. J. Appl. Phys., Part 1 **40**, 5850 (2001).
[47]C.-L. Dai, F.-Y. Xiao, C.-Y. Lee, Y.-C. Cheng, P.-Z. Chang, and S.-H. Chang, Mater. Sci. Eng., A **384**, 57 (2004).
[48]G. A. C. M. Spierings, J. B. A. Van Zon, and P. K. Larsen, Integr. Ferroelectr. **3**, 283 (1993).
[49]S. Corkovic, R. W. Whatmore, and Q. Zhang, Integr. Ferroelectr. **88**, 92 (2007).
[50]P. Padmini, R. Krawietz, R. Koehler, and G. Gerlach, Ferroelectrics **228**, 79 (1999).
[51]Z. Huang, Q. Zhang, and R. W. Whatmore, J. Appl. Phys. **85**, 7355 (1999).
[52]I. Demir, A. L. Olson, J. L. Skinner, C. D. Richards, R. F. Richards, and D. F. Bahr, Microelectron. Eng. **75**, 12 (2004).
[53]S. Choudhury, Z. Li, and L.-Q. Chen, J. Am. Ceram. Soc. **88**, 1669 (2005).
[54]PCPDF File 33-0784.